Polarization properties, high-order Raman spectra, and frequency asymmetry between Stokes and anti-Stokes scattering of Raman modes in a graphite whisker

PingHeng Tan* and ChengYong Hu
National Laboratory for Superlattices and Microstructures, P.O. Box 912, Beijing 100083, China

Jian Dong and WanCi Shen
Laboratory of Advanced Materials, Department of Materials Science and Engineering, Tsinghua University, Beijing 100084, China

BaoFa Zhang
Beijing Institute of Aeronautical Materials, P.O. Box 81-26, Beijing 100095, China

(Received 29 March 2001; revised manuscript received 13 August 2001; published 12 November 2001)

The Raman spectra of a new type of graphite whiskers have been measured in the range of 150–7800 cm^{-1}. The intensity of the overtone ($2D$) located at $\sim$2700 cm^{-1} is found to be about 10 times stronger than that of the C-C stretching mode (G) at 1582 cm^{-1}. Because of the peculiar enhancement of the $2D$ mode, high-order Raman bands up to fifth order at $\sim$7500 cm^{-1} have been observed. Polarized micro-Raman spectroscopy has been performed on an individual graphite whisker, and angular-dependent intensity measurements of all Raman modes in the VV and HV geometries are in agreement with the theoretical calculated results. Laser-energy-dependent dispersion effects and the frequency discrepancy of Raman modes between their Stokes and anti-Stokes lines in graphite whiskers are also carefully investigated. The energy dispersion of the D mode and G mode is very similar to that of highly oriented pyrolytic graphite (HOPG). In contrast to the Raman spectra of HOPG and other graphite materials, two laser-energy-dependent Raman lines are revealed in the low-frequency region of the Raman spectra of graphite whiskers, which are believed to be the resonantly enhanced phonons in the transverse-acoustic and longitudinal-acoustic phonon branches. Moreover, the obvious energy dispersion of the D' mode at $\sim$1620 cm^{-1} is observed in graphite whiskers. The results clearly reveal how strongly the peak parameters of Raman modes of graphite materials are dependent on their structural geometry. The Stokes and anti-Stokes scattering experiments show that the frequency discrepancy between the Stokes and anti-Stokes sides of a Raman mode in graphite materials is equal to the frequency value covered by the *one-phonon* energy of this Raman mode in its frequency versus laser energy curve, which is the product of the one-phonon energy of this mode ($E\omega_s$) and the value of its laser-energy dispersions ($\partial E\omega_s/\partial\varepsilon_L$).

DOI: 10.1103/PhysRevB.64.214301 PACS number(s): 63.20.Kr, 81.05.Tp, 78.30.−j, 63.50.+x

I. INTRODUCTION

Since the physical properties of graphite materials are strongly affected by their structure, Raman spectra have proved to be helpful in understanding the vibrational spectra and microstructure of graphite materials.[1–3] Polarized Raman scattering has been shown to be very useful in characterizing the geometric structure and one-dimensional characteristics of carbon nanotubes.[4,5] However up to now, the polarization effect of Raman spectra in bulk graphite crystal has not been clearly observed along the (001) crystal face[6] because of the difficulty in obtaining a well-structure-oriented (001) crystal face of graphite due to the extreme anisotropy of the forces between the atoms in graphite materials. Researches on laser-energy dispersion effects of Raman modes[7–12] and on the anti-Stokes spectra in comparison to the Stokes spectra[12,13] can give new insight into the phonon band structures and new physics about Stokes and anti-Stokes Raman scattering phenomena in graphite materials. For example, the frequency of Raman modes in many materials (diamond, silicon, etc.) is insensitive to the excitation energy, and the Stokes and anti-Stokes lines of Raman modes have equal frequency because of the demand of the energy and momentum conservation rules which have been proved by many experiments. However, it is not the case for graphite materials, such as HOPG,[12] carbon nanotubes,[13] and graphite whisker, reported here. The frequency of many Raman modes in graphite materials sensitively varies with the excitation energy and those modes have different frequencies between their Stokes and anti-Stokes lines, the physical origins of which are still under discussion.

Vapor-grown carbon whiskers have been studied extensively. Graphite layers in most of them so far prepared are curved symmetrically in cylindrical geometry and remain parallel to the whisker axis.[14–17] It is noted[18] in some rare cases that the graphite layers are aligned perpendicularly to the axis to form a ribbonlike structure with the aid of a catalyst. Recently, we synthesized a new type of graphite whisker using a high-temperature heat-treatment method,[19] whose structure is different from those of the above and whose growth does not depend on the catalyst. The new type of graphite whisker has a scale up to several μm in diameter and length. It offers the advantage to study its polarization properties and Stokes and anti-Stokes Raman scattering spectra and to investigate the laser-energy dependence of all Raman modes in graphite whiskers. Furthermore, a very strong $2D$ overtone observed in the graphite whiskers makes it possible to observe the high-order Raman bands up to fifth order at 7500 cm^{-1}. The study of the polarization effect, laser-energy dependence, and Stokes and anti-Stokes Raman scattering of Raman modes in the new type of graphite whisker enables us to identify the assignment of the observed

Raman modes and to further study the physical origin of the frequency discrepancy of certain Raman modes. The experimental results clearly reveal that the detailed peak parameters of Raman modes of graphite materials are strongly dependent on their structural geometry.

The paper is organized as follows: In Sec. II the synthesis method of graphite whiskers and the experimental arrangement of Raman scattering are described. The structure characterization of the graphite whiskers and the results of Raman-scattering experiments and discussions are presented in Sec. III. At last, conclusions are drawn in Sec. IV.

II. EXPERIMENT

Graphite whiskers were synthesized in a graphitization furnace using a high-temperature heat-treatment method at a special pressure.[19] The experiment conditions were as follows: first, natural graphite (produced in China) was ground for 24 h by a planetary mill, whose vial and balls were made up of Cr(17) stainless steel and zirconium oxide (ZrO_2), respectively. The weight ratio of balls to graphite was 30:1. The ground graphite was put into a graphite crucible with a lid, but gas can flow into it freely. The crucible was heat treated at 2100 °C, together with epoxy resins (not mixed) for 1 h in a vacuum graphitization furnace. The experiments were carried out at pressure of 30 kPa and the heating and cooling rates were 100 °C per hour. The detailed structural properties of graphite whiskers (called whiskers for short in the following text) are shown in the first part of Sec. III.

The Raman spectra of graphite whisker were recorded by the Dilor Super Labram with a typical resolution of 0.5–2 cm^{-1} in a backscattering geometry at room temperature. The system consists of a holographic notch filter for Rayleigh rejection and a microscope with 100× objective lens, allowing a spatial resolution of ~1.0 μm. The laser excitation wavelengths are 514.5 nm, 488.0 nm of an Ar^+ laser and 632.8 nm of a He-Ne laser. Typically, a low laser power of 0.1 mW arrived at the sample was used to avoid sample heating and higher power up to 2 mW was used to measure the anti-Stokes Raman signal in graphite whiskers. Polarized Raman spectra were excited with 632.8 nm excitation from almost the same spot of the same graphite whisker. We chose the $\hat{X}$ direction as the excitation laser propagation direction and recorded the backscattering signal with polarization along the $\hat{Y}$ direction. A half-wave plate was used to change the polarization direction of the incident light along either parallel (H) or perpendicular (V) to that of the scattered signal for the polarization measurement. The angle (θ) between the axis of the graphite whisker and the polarization direction of the incident laser was changed by rotating the sample manually.

III. RESULTS AND DISCUSSION

A. Structure characterization of the new type of graphite whiskers

The Raman spectra of carbon and graphite materials are known to reflect their structures very sensitively.[1,2] Before studying the Raman spectra of the new type of graphite whisker that we produced, we first discuss the structure properties of the graphite whiskers by means of transmission electron microscopy (TEM), scanning electron microscopy (SEM), and electron diffraction and x-ray diffraction (XRD) technology.

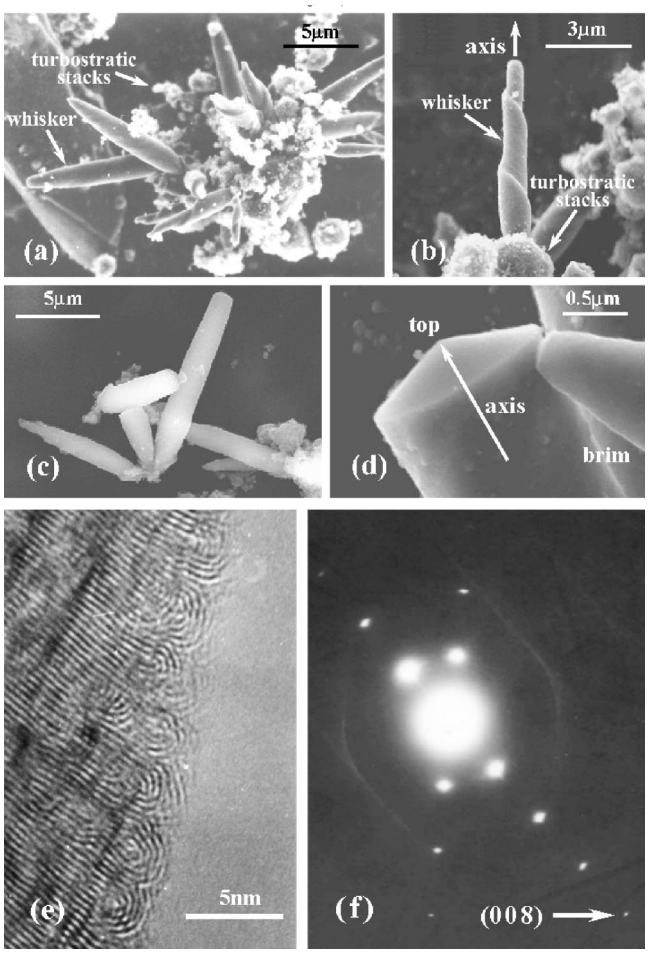

FIG. 1. SEM and TEM images and diffraction pattern of the graphite whisker prepared by the high-temperature heat-treated method. (a)–(c) Different morphologies of graphite whiskers grown on the surface of milled graphite particles. (d) A SEM image of the top region of a graphite whisker. (e) A high-resolution TEM image of the brim region close to the surface along the axis of a whisker. (f) Single-crystal electron diffraction from a graphite whisker.

Figure 1 shows several kinds of the morphology and the diffraction pattern of the graphite whisker prepared by the high-temperature heat-treated method. The whiskers grow on the surface of milled graphite particles, which lost their crystallinity after a long-time milling and then become turbostratic stacks (TS's). The diameters of the whiskers range from 0.2 to 1 μm, and their lengths range from 2 to 20 μm. The aspect ratios of length to diameter of whiskers are 5–20, which is much smaller than that of a typical carbon fiber. One of the most significant features of these whiskers is their spiral structure. The angle between the spiral face and its axis of the whisker shown in Fig. 1(b) is about 30°. More SEM images indicate that the probabilities of spirals in a

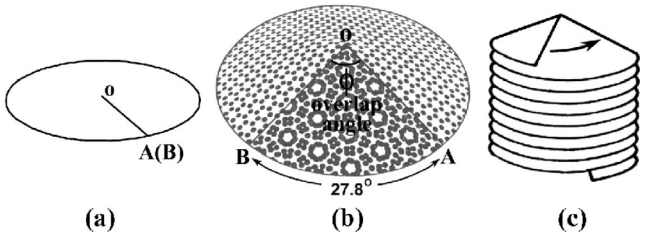

FIG. 2. The schematic diagram of the structural formation of the graphite whisker.

clockwise or anticlockwise direction seem equal to each other. The other feature that distinguishes our graphite whisker from a carbon fiber is that the changed diameter along its axis direction, as shown in Figs. 1(a)–1(c), whereas a typical carbon fiber has a uniform diameter along its axis. Figure 1(d) shows that there is a circular cone at the top of the whisker and the angle of its cone apex is about 133°. The cone tip just comes through the axis of the whisker. Most whiskers reported in other literature consist of cylindrical layers or, actually, scroll-like formations of graphite sheets extending continuously along the length of the filament, the graphite layers being oriented exactly parallel to the filament axis. However, a high-resolution TEM (HRTEM) image [Fig. 1(e)] exhibits a typical lattice image of the brim region of the whisker showing a well-ordered graphitic structure and shows that the graphite layers of the new type of graphite whisker are almost perpendicular to the whisker axis. This HRTEM image also shows that the structure of whisker brim is a frill-like one and the bending of the graphite planes in the brim of whisker eliminates the dangling bands, which makes the bent graphitic layers look like multiple-walled nanotube tips in the cross section. The spiral structure, cone tip, and the existence of the acute angle between graphite layers and the whisker axis suggest that the whiskers may be composed of the conical spiral structure of graphite layers. Figure 2 illustrates the schematic diagram of the structural formation of this new type of graphite whiskers, and the detailed growth mechanism of the spiral formation of graphite whiskers has been described elsewhere. The overlap angle (ϕ) between two radii OA and OB determines the cone angle (γ) as the expression of $\phi=2\pi[1-\sin(\gamma/2)]$. The cone angle of 133° observed in Fig. 1(d) can lead to a overlap angle of 29°. The theoretical calculation shows that two overlapped graphite layers can produce an interesting atom picture [Fig. 2(b)] if the overlap angle is 27.8° and the cone angle is 135°, which is in agreement with the experimental observations. The electron diffraction pattern from the graphite whisker [Fig. 1(f)] confirms the above conclusions. In Fig. 1(f), there are two sets of $(00l)$ spots, one of which even exhibits the diffraction spots up to the (008) spot, which shows that the graphite whisker has a high degree of crystalline order. The two sets of diffraction patterns correspond to the two sets of chevroned graphite layers in the cone whisker structures. Based on this structural configuration of the whisker, we can calculate that the interlayer spacing is about 0.34 nm and the angle between the graphite layers and the axis is about 67.5° from Fig. 1(f), which is consistent with the observed cone angle of 133°.

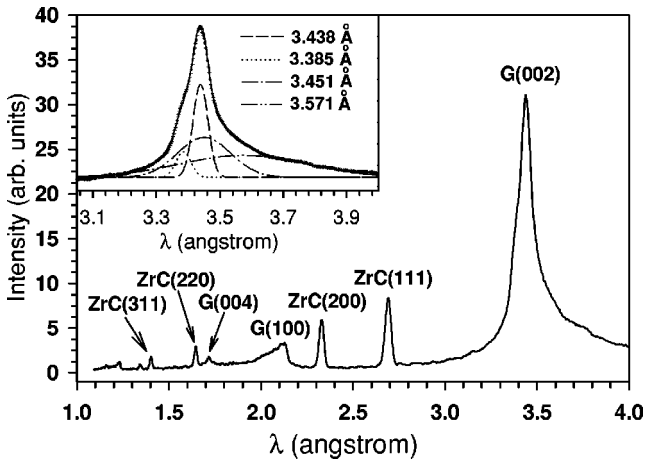

FIG. 3. X-ray diffraction analysis of the powder sample mixed with the graphite whisker and the milled graphite particles. The inset shows four Gaussian peaks used to fit the (002) peak of the powder sample.

The x-ray diffraction pattern of the mixed powder that contains the graphite whisker and the milled graphite particles is shown in Fig. 3. The diffraction peaks located at 0.344, 0.210, and 0.172 nm are known as the (002), (100), and (004) peaks of graphite crystals. At least four different Gaussian peaks that located at 0.3385, 0.3438, 0.3451, and 0.3571 nm are necessary to give a good fit to the experimental data of the (002) peak of the mixed powder. The 0.3451 and 0.3571 nm peaks may be related to the diffraction peaks of disorder graphite materials (e.g., turbostratic stacks in the graphite particles),[20] because x rays cannot be focused on to a single graphite whisker. The 0.3385 and 0.3438 nm peaks are believed to be the diffraction peaks of the graphite whisker. The interplanar spacing of <0.344 nm suggests that the graphite whisker is highly graphitized as shown in Fig. 1(e). Except the diffraction peaks of graphite materials, other peaks labeled in Fig. 3 are in agreement with those of a ZrC crystal.[21] Because mill balls were made up of zirconium oxide (ZrO_2), the ZrC crystal will be formed when the ZrO_2 fragment that is mixed into the graphite powder in the milling is heat treated at 2100°C. There is no diffraction peaks of other materials except those of graphite materials and ZrC crystals.

B. Overview of the spectral characteristics of the Raman spectra in graphite whiskers

A wide range of aspect ratios of graphite whiskers enables us to find them under the microscope and to record the Raman spectra of an individual graphite whisker. Figure 4 shows the Raman spectra of a graphite whisker in the range of the first- and second-order regions using the 632.8 nm laser excitation.

Single-crystal graphite belongs to the D_{6h} symmetry group, and the irreducible representation for optical modes in the Brillouin zone center is given by[1]

$$G_{opt}=2E_{2g}+E_{1u}+2B_{2g}+A_{2u}. \quad (1)$$

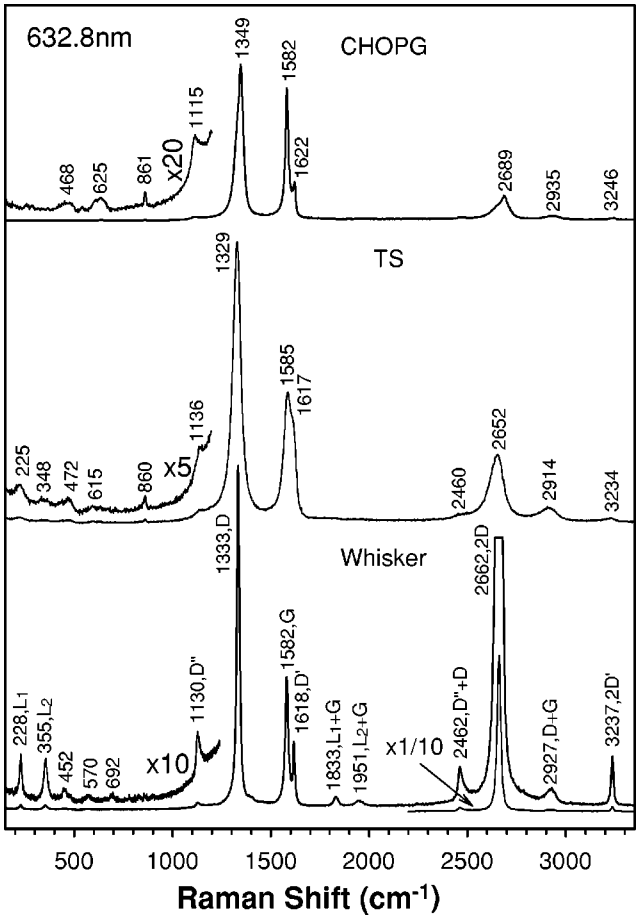

FIG. 4. Raman spectra of C^+-implanted highly oriented pyrolytic graphite, turbostratically stacked (TS) structures, and a graphite whisker in the range of the first- and second-order regions.

The first-order Raman spectrum of highly oriented pyrolytic graphite (HOPG) shows a strong band, which has been assigned to the in-plane E_{2g} zone-center mode, at $\sim$1582 cm^{-1} (G).[1] In the C^+ ion-implanted HOPG (CHOPG) and microcrystalline graphite, additional first-order lines appear at $\sim$1333 cm^{-1} (D) and $\sim$1618 cm^{-1} (D'), which have been assigned to noncenter phonons and to fundamentals corresponding to the high density of phonon states.[1,2,22] Those modes and their overtones [at $\sim$2662 cm^{-1} $(2D)$ and $\sim$3237 cm^{-1} $(2D')$] and combinations [at $\sim$2927 cm^{-1} $(D+G)$] have been observed in the Raman spectra of graphite whiskers. As well as the D mode, the mode at about 1130 cm^{-1} that is forbidden and not observed in the single-crystal graphite becomes Raman active in graphite whiskers due to the selection-rule relaxation resulting from finite-crystal-size effects and defects.[12] For convenience in referring to this mode, we designate it as D'' in the following text. The line shape of the 1130 cm^{-1} (D'') mode is very similar to that of the mode at 2462 cm^{-1}, and the sum of the frequency of the D'' and D modes in the graphite whisker is very close to that of 2462 cm^{-1} mode, and therefore, the 2462 cm^{-1} mode can be assigned to the combination of the D mode and D'' modes as the assignment of the mode at 2465 cm^{-1} in HOPG and CHOPG.[12]

Figure 4 also shows Raman spectra of TS's along with that of CHOPG, in which all spectra are normalized to the intensity of the G mode. Compared with those of CHOPG and TS's, the Raman spectra of whiskers have several distinct characteristics. First, the intensity of the $2D$ overtone is found to be 13 times stronger than that of the first-order G mode in whiskers, while that of the $2D$ mode in CHOPG and HOPG excited by 632.8 nm laser excitation is only one-fifth and one-half of the G mode,[12] respectively. At the same time, the $2D'$ and the mode at 2462 cm^{-1} in whiskers also show a stronger intensity than the corresponding modes in CHOPG and TS's. Second, although the intensity ratio of the D band to the G band is up to 2.8, which is larger than (2.3) of TS's, many modes of whiskers still exhibit smaller linewidths (full width at half maximum intensity) than those of TS's. For example, the linewidth of the D, G, D', $2D$ and $2D'$ in whiskers (TS's) are 17 (48), 18 (46), 10 (27), 20 (75), and 14 (70) cm^{-1}, respectively. The linewidth of the G mode in whiskers is slightly larger than that of the G mode in HOPG. The small linewidth of Raman lines in whiskers indicate that the whisker has very good crystal quality, which is indicated by the HRTEM image [Fig. 1(e)] and electron diffraction pattern [Fig. 1(f)] of graphite whiskers. Moreover, there are two additional sharp peaks in the Raman spectra of whiskers located in the low-frequency region at 228 cm^{-1} (L_1) and 355 cm^{-1} (L_2), and two additional strong modes (1833 and 1951 cm^{-1}) appear at the second-order frequency region. According to the frequency match, the 1833 and 1951 cm^{-1} modes are assigned to combination modes of L_1+G and L_2+G, and other three additional peaks observed at 452, 692, and 570 cm^{-1} are designated as the overtones of the L_1 and L_2 modes and the combination of L_1 and L_2 modes, respectively. The physical candidates for the two special L_1 and L_2 modes will be discussed in the fourth part of Sec. III.

Usually, the intensity of the 2D mode is about half as much as that of the G mode in HOPG and in the side surface of graphite polyhedral crystals (GPC's). However, the enhancement intensity of the $2D$ mode has also been observed in the Raman spectra from the crystal tip of GPC's, in which the intensity of the $2D$ mode is almost equal to that of the G mode.[17] The electron microscopy micrograph of GPC's (Ref. 17) shows the semicylindrical termination of graphite planes in the crystal tip region and bent graphitic layers look like two-layer nanotube tips in the cross section, which is very similar to the structural characteristics of the brim region of the whisker close to the surface along its axis. However, the intensity enhancement of the $2D$ mode relative to the G mode is not observed from HOPG and the side face of GPC's, whose structure close to the surface is a well-ordered graphitic structure and whose Raman spectrum corresponds to perfect graphite with a narrow G mode and no D mode, similar to that from HOPG. Thus, the peculiar structure of the whisker or filament, which the curved termination of the graphite sheets make the most of free edge carbon atoms disappear and eliminate the dangling bonds in the brim region, is believed to produce the unusual strong enhancement of the 2D mode in those graphite materials.

The Raman characteristics of TS's are somewhat similar to those of a whisker, and the assignment of many Raman bands of TS's can refer to that of the corresponding modes in a whisker. Because TS's contain much structural disorder and has a much smaller crystallite planar size than the whisker,[21] their Raman spectra exhibit weakened and broadened peak widths. For instance, two weak peaks appear in the Raman spectra of TS's at the corresponding positions of the L_1 and L_2 modes in whiskers. Other two weak and broad peaks of TS's at $\sim$472 and $\sim$615 cm^{-1} originate from the vibrational modes in CHOPG located at $\sim$468 and $\sim$625 cm^{-1}, which may be the fundamentals corresponding to the high density of phonon states. A new Raman peak at about 861 cm^{-1} is observed in CHOPG and TS's, which do not appear in the Raman spectra of HOPG. The frequency of this peak is lower than that (868 cm^{-1}) of the A_{2u} mode[1] observed in the edge plane of HOPG,[6] and therefore, it cannot be assigned as the out-of-plane A_{2u} mode. This mode may also be the fundamentals corresponding to the high density of phonon states.

The intensity ratio of the *D* band to the *G* band has been reported to be inversely proportional to the crystallite planar size.[23] The intensity ratio of the *D* band to the *G* band (I_D/I_G) in CHOPG, TS's and graphite whisker is 1.2, 2.3, and 2.8. This indicates that a graphite whisker has a smaller crystallite planar size, which should induce broadening in all Raman modes and weakening of the overtones and combination modes in graphite materials.[2,24] However, the peak width of the *D* mode in a graphite whisker is very narrow and close to that of the *G* mode in HOPG. High-resolution electron microscopy images [Fig. 1(e)] also show that graphite whiskers are highly graphitized and have very good crystal quality. Thus, the results suggest that there exists a special enhancement factor on the *D* mode (also the 2*D* mode) in whiskers so that the intensity ratio of the *D* band to the *G* band cannot be used to estimate the crystallite planar size of the graphite whisker.

C. Orientation-dependent Raman spectra of graphite whiskers

Theoretical calculation shows that, not only the symmetry but also the direction of the normal mode displacements is important in determining the polarization intensities, and the intensity in the different scattering configurations can be used to identify the symmetry assignments for some of the Raman-active modes. For the graphite materials, the polarization effect of Raman modes has been used to confirm the observation of the out-of-plane A_{2u} mode at 868 cm^{-1}.[29] However, the investigation of the polarization effect of Raman modes in graphite materials is limited by the degree of the crystal quality because the disorders and defects in the materials play an important role in the Raman spectra of graphite materials.[1,2] This can explain why the intensity of the *G* mode obtained with the incident light polarized perpendicular to the graphite plane is one-fourth as much as those with the incident light polarized parallel to the plane, but is not equal to zero as the theoretical predictions.

The high degree of the crystal quality, the peculiar structure of the conical graphite layers, and the wide range of aspect ratios and diameters of graphite whiskers offer us an advantage to investigate the polarization properties of graphite whiskers.

The intensity of a phonon mode for a given scattering geometry can be determined from the polarizability tensors. The *G* mode at $\sim$1582 cm^{-1} exhibits E_{2g} symmetry; its Raman polarizability tensors are given by[25]

$$E_{2g}(1)\rightarrow\alpha_1=\begin{bmatrix} 0 & -d & 0 \\ -d & 0 & 0 \\ 0 & 0 & 0 \end{bmatrix}, \tag{2}$$

$$E_{2g}(2)\rightarrow\alpha_2=\begin{bmatrix} d & 0 & 0 \\ 0 & -d & 0 \\ 0 & 0 & 0 \end{bmatrix}. \tag{3}$$

The Raman polarizability tensors determine the intensity of the Raman mode with E_{2g} symmetry scattered from the sample according to

$$I_R\propto\sum_i |\hat{e}_s\cdot\alpha_i\cdot\hat{e}_L|^2, \tag{4}$$

where $\hat{e}_L$ and $\hat{e}_s$ are the unit polarization vectors of the incident and scattered light, respectively. We fixed the $\hat{X}$ direction as the excitation laser propagation direction, then recorded the backscattering signal with the polarization along the $\hat{Y}$ direction with unit vectors $\hat{e}_s=(0\ 1\ 0)$, and denoted this axis as the *V* direction. By using a half-wave plate, the polarization of the incident excitation is turned to parallel [$(V,\ \hat{e}_{L\parallel}=(0\ 1\ 0))$ and perpendicular $[H,\ \hat{e}_{L\perp}=(0\ 0\ 1)]$ to $\hat{e}_s$. Considering the fact that graphite layers are not strictly perpendicular to the whisker axis, the angle φ is introduced to the existent angle (67.5°) between graphite layers and the whisker axis. When defined the oriented angle of the whisker axis with respect to the $\hat{y}$ axis (in the *yz* plane) as θ, the last expressions given for the angle-dependent scattering intensity of the Raman signal for the *VV* and *HV* scattering configurations, respectively, are

$$I_{VV}(\varphi,\theta)=I_0\cdot[\cos^2\varphi\cos^2\theta+\sin^2\theta]^2, \tag{5}$$

$$I_{HV}(\varphi,\theta)=I_0\cdot[\cos^4\varphi\cos^2\theta\sin^2\theta+\cos^2\varphi(\cos^4\theta+\sin^4\theta)+\cos^2\theta\sin^2\theta]. \tag{6}$$

The relative intensity of the Raman signal for the *VV* configuration to that for the *HV* configuration is usually defined as the depolarization ratio:[25]

$$\rho(\varphi,\theta)=I_{VV}(\varphi,\theta)/I_{HV}(\varphi,\theta). \tag{7}$$

Figure 5 shows the polarized Raman spectra of a graphite whisker measured for the *VV* and *HV* scattering configurations when the axis of the graphite whisker is aligned perpendicular to the polarization of the scattered light ($\theta=90°$) as shown in the inset of Fig. 5. Because the diffraction pattern shows that the angle between the graphite layers and the whisker axis is 67.5°, the calculated depolarization

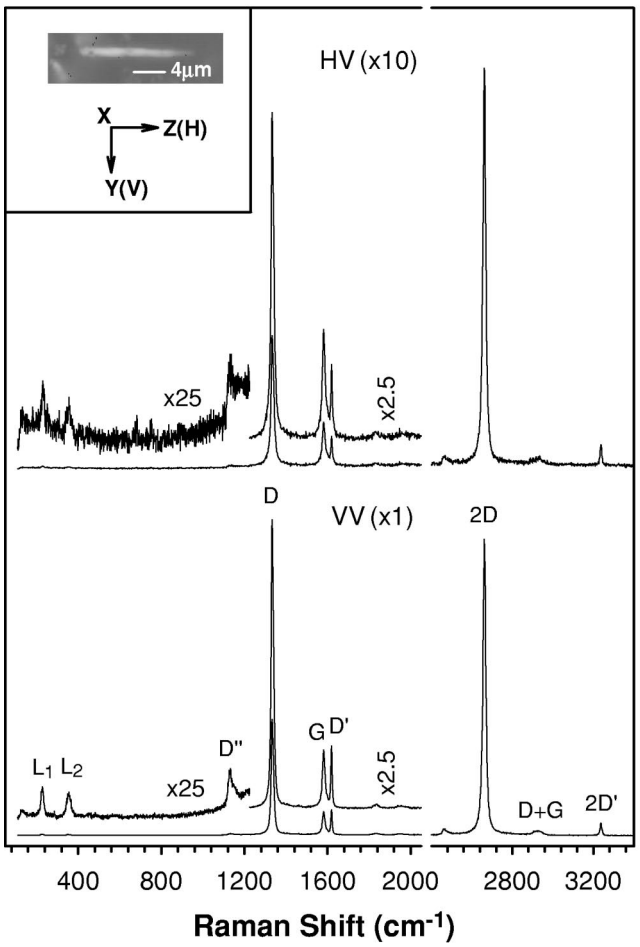

FIG. 5. Raman spectra of a graphite whisker in the range of the first- and second-order regions in the *VV* and *HV* scattering configurations, while the whisker axis is aligned perpendicular to the polarization of the scattered light ($\theta=90°$). The inset shows the optical microimage of the measured whisker and the set of three mutually perpendicular coordinate axes.

ratio of the *G* mode, $\rho_G(67.5°, 0°)$, is equal to 6.8, which is very close to the experimental value of 5.8. Another interesting result is that the depolarization ratios of the *D* and *D′* modes and their overtones 2*D* and 2*D′* modes are 9.0, 10.0, 7.6, and 6.0, respectively, which are larger than that of the *G* mode with E_{2g} symmetry. Thus, the intensities of almost all Raman bands in the spectrum obtained with the polarization direction of the incident excitation perpendicular to the whisker axis are much stronger (about 6–10 times) than those with the polarization direction of the incident excitation parallel to the whisker axis, although graphite layers in whiskers are not strictly perpendicular to the whisker axis. The high depolarization ratios of L_1 and L_2 modes and of two modes at 1833 and 1951 cm^{-1} (see Fig. 2) also confirm that they are the intrinsic modes of graphite whisker other than the modes arising from impurities.

We measured the Raman spectra of a graphite whisker in the VV and HV configurations for various angles θ. Figure 6 displays Raman spectra in the *VV* and *HV* configurations with different angles θ between the polarizations of the scattered light and the whisker axis. In the measurement, the axis of the whisker is rotated manually and its oriented angle θ is calculated from the optical microimage obtained from the digitized camera. For the *VV* configuration, all Raman modes show a maximum intensity when the polarizations of the incident laser light with no use of half-wave plate is perpendicular to the whisker axis ($\theta=90°$), while near $\theta=0°$ all Raman modes reach a minimum intensity. However, for the *HV* configuration, all Raman modes show a minimum intensity when the polarizations of the incident laser light with no use of half-wave plate is perpendicular or parallel to the whisker axis ($\theta=90°$ or $0°$), while near $\theta=45°$ the intensity of all Raman modes reaches a maximum value. Those angular dependence of Raman modes in graphite whiskers were fully reproducible for all of the individual graphite whiskers in the sample.

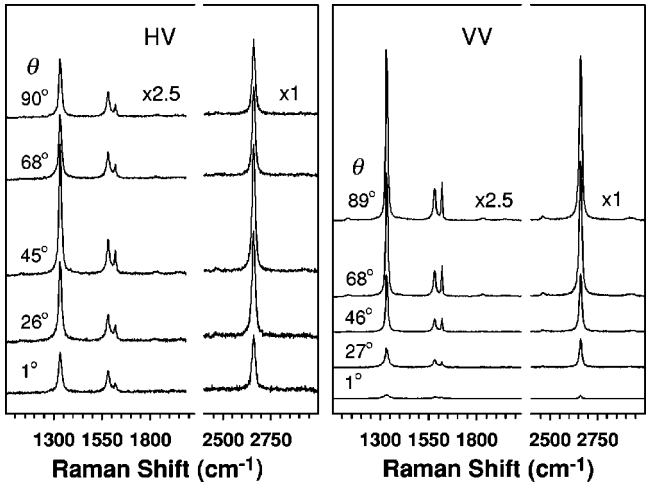

FIG. 6. Raman spectra of the *D*, *D′*, 2*D*, and 2*D′* modes of a graphite whisker in the *VV* and *HV* configurations for different angles θ between the polarizations of the scattered light and the whisker axis. For $\theta=0°$, the polarization of the incident excitation with no use of half-wave plate is parallel to the axis of the graphite whisker.

The detailed angular dependences of the intensities of the *D* and *D′* modes and their overtones 2*D* and 2*D′* modes for *VV* and *HV* configurations are shown in Fig. 7. The group theory predictions based on Eq. (5) and Eq. (6) are also drawn in Fig. 7 with solid lines. The calculated results are qualitatively consistent with experimental data, which suggests that almost all bands in the spectrum of graphite whisker exhibit E_{2g} symmetry. In contrast to the *G* mode, the *D*, *D′*, and 2*D* modes have stronger polarization and are better in agreement with the E_{2g} symmetry predictions. The whisker is composed of many conical graphite layers, but no graphite layers parallel to the whisker axis. Because the diameter of the probed whisker is 1.4 μm and the spatial resolution of the Raman system is $\sim$1.0 μm, the measured graphite layers are actually somewhat curved graphite layers. Therefore, the distinct structural characteristic of graphite whiskers results in a small discrepancy between the observed depolarization ratio of the *G* mode in whiskers and the E_{2g} symmetry prediction.

Kawashima and Katagiri[6] reported that the *D* and *G*

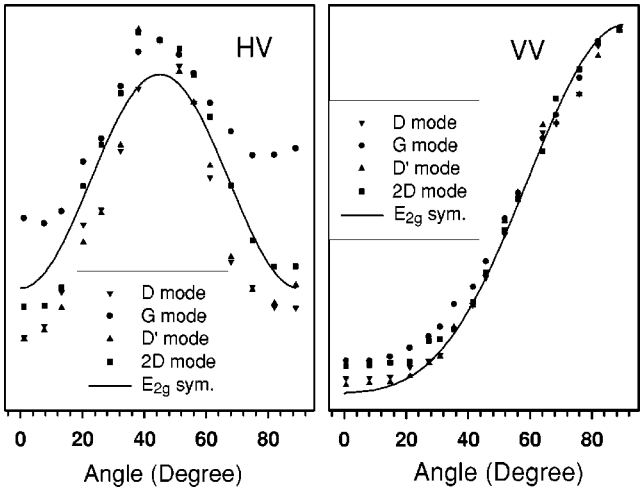

FIG. 7. Angular dependence on the intensities of D, D', $2D$, and $2D'$ modes of a graphite whisker in the VV and HV configurations.

modes have almost the same depolarization ratio for the edge plane of HOPG; however, Compagnini and Baratta[26] found different depolarization ratios between the D and G modes of ion-irradiated HOPG and interpreted this result by an anisotropic damage induced in the HOPG structure by an ion collision cascade. After checking the experimental results (Figs. 5–7) of the polarized spectra of graphite whiskers, one can find that it is a general phenomenon for the different depolarization ratios between the D and G modes in the graphite whisker. It is the same case for HOPG. Figure 8 shows the polarized Raman spectra of HOPG and C^+-ion-implanted HOPG (CHOPG) with the polarization of the incident and scattered lights parallel to the graphite layers, where the C^+ ion beam was normally directed to the graphite c face with a dose of 1.0×10^{14} ions/cm^2 at an accelerating voltage of 100 keV. The depolarization ratio of the G mode of HOPG and CHOPG is 1.02 and 1.04, respectively, which is very close to the value $\rho(0,\theta)$ $(=1.0)$ of the group theory predictions based on Eq. (5) and Eq. (6). However, the depolarization ratios of other modes in HOPG and CHOPG are greater than 2.0. Table I summarizes the depolarization ratios of all Raman modes relative to that of the G mode in HOPG, CHOPG, and whiskers. Because the overtone of the D mode observed in HOPG and whiskers has a different polarization effect than the G mode, therefore, the discrepancy between the depolarization ratio of the G mode and D modes is an intrinsic property of graphite materials. The D, D', and D'' modes of graphite materials originate from the Raman scattering of the noncenter optical phonons in the Brillouin zone; therefore, those modes are not purely optic or acoustic, transverse or longitudinal, but rather have a mixed character.[27] The dependence of the frequency of the D and D'' modes on the laser energy indicates that the D and D'' modes are resonantly excited phonon modes in the Brillouin zone by a resonant coupling of the excitation laser with electronic states of graphite materials, and the breakdown of Raman selection rules is a well-known effect for resonant Raman scattering.[28] All these factors can result in a different depolarization ratios between the G mode and other modes (D'', D, D', $D+G$, $2D'$, etc.) in HOPG, CHOPG, whiskers, and other graphite materials.

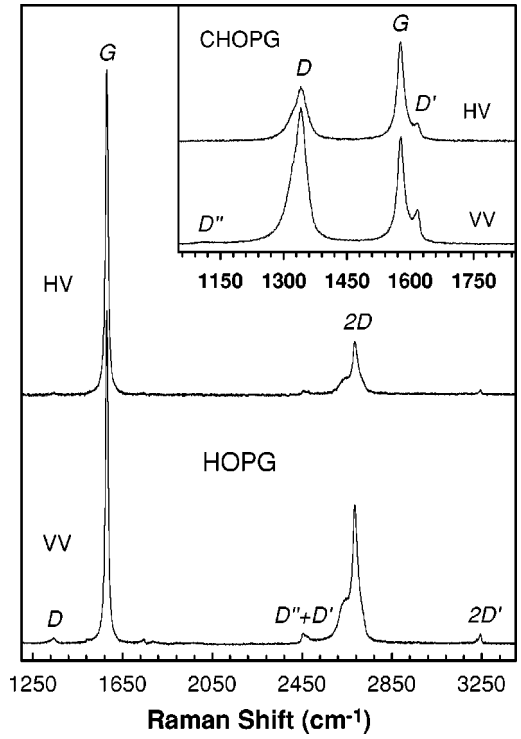

FIG. 8. Polarized Raman spectra of HOPG and C^+-ion-implanted HOPG in the VV and HV scattering configurations with the polarization of the incident and scattered light parallel to the graphite layers.

D. High-order Raman bands and dispersion effects in graphite whiskers

Figure 9 shows the Raman spectra of a graphite whisker in the range of 100–7800 cm^{-1} excited by 488.0 nm, 514.5 nm, and 632.8 nm laser excitations. Besides the above assignments of the first-order and second-order Raman modes, many high-order Raman modes, such as at 4052, 4300, 4549, 4853, 5392, 5638, 5879, 6953, and 7478 cm^{-1}, have been observed in the Raman spectra excited with 488.0 nm excitation. Based on the assignment of the corresponding modes in other carbon materials[29–31] and their frequency matches and intensities, we designate the 4052, 4300, 4549, 4853, 5392, 5638, 5879, 6150, 6443, 6953, and 7478 cm^{-1} bands as $3D$, $2D+G$, $D+2G$, $3D'$, $4D$, $3D+G$, $2D+2G$, D

TABLE I. The relative depolarization ratios of all Raman modes to the G mode in HOPG, CHOPG, and whiskers for scattering configurations with the polarization of the incident and scattered lights parallel to the graphite layers of HOPG and CHOPG, and with the scattered light perpendicular to the whisker axis.

Assignment	D_1	D_2	G	D'	$D''+D$	$2D_1$	$2D_2$	$D+G$	$2D'$
HOPG	-	-	1.0	-	2.7	2.8	2.6	-	2.3
CHOPG	3.2	2.4	1.0	2.2	2.3	2.2	2.0	1.8	2.1
Whisker	1.6		1.0	1.7	1.3	1.3		1.2	1.0

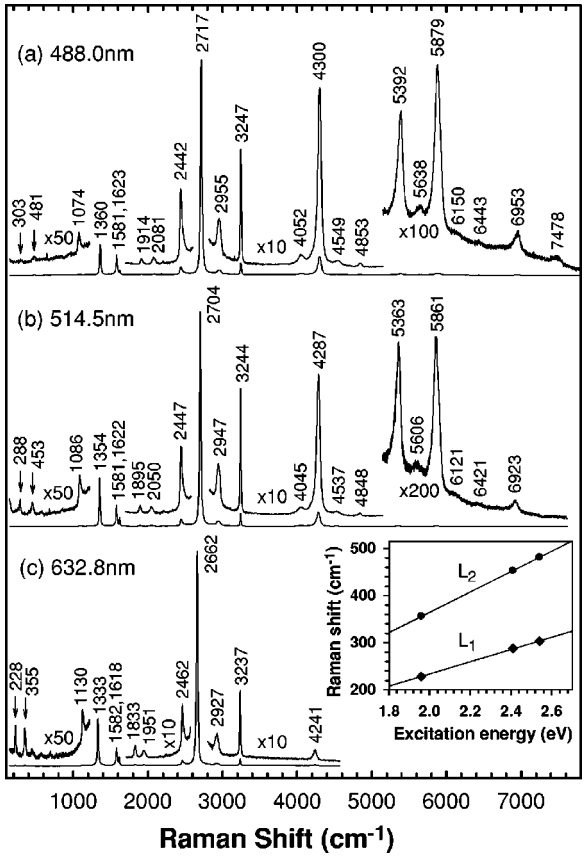

FIG. 9. Raman spectra of a graphite whisker with (a) 488.0 nm, (b) 514.5 nm, and (c) 632.8 nm laser excitations. The inset gives the energy dispersion of the two modes labeled with arrows.

$+3G$, $4D'$, $4D+G$ and $2D+3G$ modes, respectively. The assignments of the main fundamental and higher-order modes of a whisker excited by 488.0 nm excitation are summarized in Table II.

The observation of the high-order Raman modes is limited by the crystalline quality. High-order Raman scattering up to fourth-order modes at 5898 cm^{-1} with 488.0 nm excitation has been observed in highly oriented pyrolytic graphite,[29,31] and the strong resonant enhancement effect makes it possible to observe up to fifth-order Raman scattering in single-walled carbon nanotubes[31] (e.g., up to Raman shifts of 6885 cm^{-1} using 488.0 nm excitation). However, in a graphite whisker, many high-order Raman modes up to the fifth-order mode at 7478 cm^{-1} are clearly revealed, and high-order Raman modes of whiskers have narrower peak width and have much stronger intensities relative to the corresponding G mode than those of other carbon materials, such as pyrolytic graphite[29] and carbon nanotubes.[30,31] This indicates that the microstructure of graphite whisker is composed of many crystalline domains with a high degree of crystalline order. It is undoubtedly that the high crystalline quality of graphite whiskers [see Figs. 1(e) and 1(f)] and the strong enhancement of the $2D$ mode in the graphite whisker help to detect the higher-order Raman spectra.

Since the D and $2D$ modes involve a different resonance process than the G mode of graphite materials, the D and $2D$ modes show different properties in graphite materials; for example, the D and $2D$ modes have a strong dispersion effect that their frequencies vary with the energy of laser excitations.[3,7–12] Table II lists the theoretically predicted frequencies and energy dispersions of all observed Raman modes in whiskers based on the experimentally observed frequencies (ω) excited with 488.0 nm excitation and the dispersion $\partial\omega/\partial\varepsilon_L$ of D, G, and other fundamentals (here ε_L is the laser energy). For example, $\omega_D = 1360$ cm^{-1}, $\omega_G = 1581$ cm^{-1}, $\omega_{D'} = 1624$ cm^{-1}, $\partial\omega_D/\partial\varepsilon_L = 46$ cm^{-1}/eV, and $\partial\omega_G/\partial\varepsilon_L = \partial\omega_{D'}/\partial\varepsilon_L = 0$ cm^{-1}/eV. The large dispersion of the D mode and other modes and the absence of dispersion for the G mode are key factors in the identification of the overtones and combination modes in Table II. For instance, the energy dispersions of the modes at 1914 and 2081 cm^{-1} ($\varepsilon_L = 2.54$ eV) are very close to those of the lowest two bands at 303 and 481 cm^{-1} labeled with arrows in Fig. 9. This result confirms the combination assignment of 1914 and 2081 cm^{-1} modes according to the frequency match.

Table II shows that the observed frequencies and their dispersions of the second-order Raman modes are in good agreement with the value predicted from the mode assignments and from the frequencies and dispersions for the D and G modes. The frequencies and dispersions of the high-order

TABLE II. The assignments of main fundamentals and higher-order modes of a graphite whisker excited by 488.0 nm laser excitation, and the overview of the experimental (*expt*-) and theoretical (*th*) values for the peak positions ω (cm^{-1}) and their dispersions $\partial\omega/\partial\varepsilon_L$($cm^{-1}$/eV) of the fundamentals and their overtones and combination modes where ε_L is the excitation energy.

ω_{expt} (cm^{-1})	Assignment	ω_{th} (cm^{-1})	$(\partial\omega/\partial\varepsilon_L)_{expt}$ (cm^{-1}/eV)	$(\partial\omega/\partial\varepsilon_L)_{th}$ (cm^{-1}/eV)
303	L_1		129	
481	L_2		216	
1074	D''		-96	
1360	D	1360	46	46
1581	G	1581	0	0
1623	D'	1624	9	0
1914	L_1+G	1884	140	129
2081	L_2+G	2062	224	216
2442	$D''+D$	2435	-35	-50
2717	$2D$	2720	95	92
2955	$D+G$	2942	48	46
3247	$2D'$	3248	18	0
4052	$3D$	4083	49	138
4300	$2D+G$	4303	99	92
4549	$D+2G$	4523	92	46
4853	$3D'$	4872	38	0
5392	$4D$	5444	221	184
5638	$3D+G$	5664	244	138
5879	$2D+2G$	5884	137	92
6150	$D+3G$	6103	221	46
6443	$4D'$	6496	168	0
6953	$4D+G$	7025	229	184
7478	$2D+3G$	7465		92

combination modes of the $2D$ mode (e.g., $2D+G$, $4D$, $2D+2G$, $4D+G$, etc.) are qualitatively consistent with the predicted values, but those of the $D+2G$, $3D+G$, and $D+3G$ modes show a large discrepancy from the values of theoretical calculations. The D mode arises from the Raman scattering of the noncenter optical phonons in the Brillouin zone; however, the $2D$ overtone can satisfy the wave-vector selection rule with zero wave vector by the combination of two D modes with equal and opposite wave vectors on the same branch of the dispersion curves, and thus, the high-order combination modes of the $2D$ mode and the zone-center G mode can easily satisfy the wave-vector selection rule and exhibit a strong intensity; their dispersions can also be consistent with the predicted values from that of the $2D$ mode. For the $D+2G$, $3D+G$, and $D+3G$ modes, they can become Raman active by the combination of the G modes with nonzero wave vector to satisfy the wave-vector selection rule, where the $2G$, $3D$, and $3G$ components in the $D+2G$, $3D+G$, and $D+3G$ modes may be contributed from phonons with different wave vector or on different branches of the dispersion curves. Here, we do not consider the relaxation of wave-vector conservation due to some kinds of crystalline imperfection degrading the translational symmetry, because the disorders and defects do not help to observe the Raman modes up to the third-order and fourth-order modes. Therefore, the observed frequencies and dispersions of the $D+2G$, $3D+G$, and $D+3G$ modes do not follow those of the fundamentals.

The dispersion behaviors of D and D' modes are very different from each other in CHOPG.[12] The frequency of the D' mode and of its overtone $2D'$ is almost insensitive to the excitation energy while the dispersion of the D mode is about $\partial\omega/\partial\varepsilon_L = 45\ \mathrm{cm}^{-1}/\mathrm{eV}$.[12] Unlike the weak shoulder structure of the D' mode beside the G mode in CHOPG and pyrolytic graphite,[12,29] the G mode and D' mode in graphite whiskers are completely separated into two independent peaks because of their narrow peak widths, so that the peak position of the D' mode can be precisely determined in the graphite whisker. The result shows that the frequencies of D', $2D'$, and $3D'$ modes in graphite whisker are obviously changed with the excitation energy and the dispersion of D' is about $10\ \mathrm{cm}^{-1}/\mathrm{eV}$. This gives experimental evidence for the dispersion effect of the D' mode in some forms of graphite materials.

As described above and in the other literature, the frequency of the D and D'' modes in the Raman spectra of CHOPG and graphite whiskers is strongly dependent on the energy of the laser excitation.[12] Recently, some mechanisms based on the single- or double-resonant Raman process have been proposed to understand the excitation-energy dependence of the D mode in graphite materials.[9–11] In contrast to the blueshift of the D mode, the D'' mode redshifts to the low-frequency region with increasing the excitation energy. According to the calculated phonon dispersion curves and electronic energy bands of $2D$ graphite[9,10] and the frequency dependence on the excitation energy, the D'' mode may be attributed to the resonant Raman scattering of the opposite dispersion of the phonon branch away from the K point that associates with the low-frequency TA phonon branch indicated by heavy lines in Fig. 3 of Ref. 10.

Compared with Raman spectra of other graphite materials,[1,8,12,22,29] graphite whiskers exhibit two intrinsic modes located at $228\ \mathrm{cm}^{-1}$ (L_1) and $355\ \mathrm{cm}^{-1}$ (L_2) for $E_{laser} = 1.96$ eV which are strongly dependent on the excitation energies and have the same polarization behavior as the G mode with E_{2g} symmetry. The two modes cannot be attributed to the features associated with the phonon density of states because there is no existence of such peaks in the theoretically calculated phonon density of states.[2] The laser-energy-dependent D mode is believed to be the resonantly enhanced phonons that are at the same distance Δq from the K point as the electronic states at Δk that are in resonance with the laser energy.[10,32] It is well known that the acoustic phonon branches in graphite are strongly coupled to the high-frequency optic branches at the K point.[27,33] Therefore, it should be possible to couple the electronic states at Δk from the K point with the phonons with wave vector Δq from the Γ point in the acoustic phonon branches, and thus, these phonons in the acoustic phonon branches are selectively probed by the resonant Raman process. To check this thought, a plot of the peak Raman frequency for the L_1 and L_2 modes versus laser excitation energy is shown in the inset to Fig. 9. Two lines can be well fitted to the data with the slopes of 129 and $216\ \mathrm{cm}^{-1}/\mathrm{eV}$ for the L_1 and L_2 modes, respectively, and the ratio (0.60) of the two slopes for L_1 and L_2 modes is almost equal to that (0.59) of the sound velocities (v_{TA}, v_{LA}) of the TA and LA phonon branches around the Γ point based on the experimental values[34,35] of $v_{TA}^{G3D} = 12.3$ km/s and $v_{LA}^{G3D} = 21.0$ km/s in three-dimensional graphite. In this point, the laser-energy-dependent L_1 and L_2 modes are believed to be the resonantly enhanced phonons in the TA and LA phonon branches. The two resonantly selective modes observed at the low-frequency region may be helpful to designate the new laser-energy-dependent combinations in the region of 1800–2300 cm^{-1} observed in pyrolytic graphite[29] and carbon nanotube.[13,31]

E. Anti-Stokes Raman spectra of graphite whiskers

Figure 10 shows Stokes and anti-Stokes Raman spectra of graphite whisker excited by 632.8 nm excitation. For the convenience of comparing the Stokes and anti-Stokes spectra with each other, the anti-Stokes spectra in Fig. 10 have been multiplied by the theoretically predicted factor I_s/I_{as} of the intensity ratio of the Stokes to anti-Stokes signals at the distinct temperature T of the sample,

$$I_s/I_{as} = \left[\frac{\omega_{las}-\omega}{\omega_{las}+\omega}\right]^4 \exp(\hbar\omega/k_B T), \tag{8}$$

where ω and ω_{las} are the frequency of Raman line and laser excitation, and k_B is Boltzmann's constant, respectively. The sample temperature determined from the anti-Stokes/Stokes Raman intensity ratio of the G mode is about 550 K, and the temperature dependence of the G mode in the whisker is $-0.021\ \mathrm{cm}^{-1}/\mathrm{K}$, which is larger than that in HOPG and smaller than that in CHOPG.[36] The temperature dependence

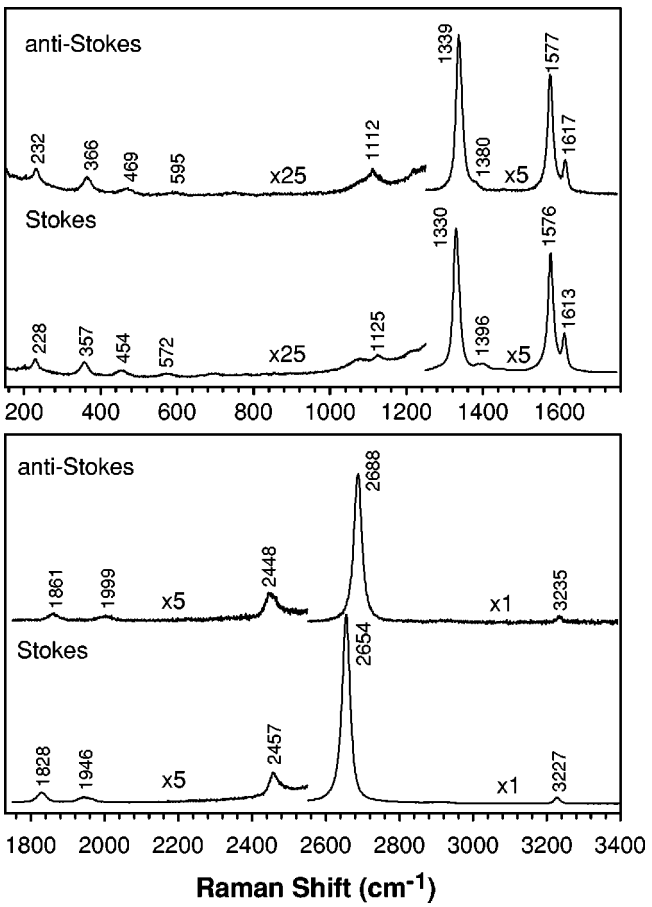

FIG. 10. The Stokes and anti-Stokes Raman spectra of a graphite whisker excited by 488.0 nm excitation. The anti-Stokes Raman spectra have been multiplied by a correction factor I_s/I_{as} defined in the text and are drawn with the x scale of the Stokes spectra for convenience in comparing them with each other.

of the G mode in graphite materials is related to their finite crystal planar domain size caused by defects and impurities.[36] The shorter the crystal planar domain size is, the easier the crystal planar domain expands with the temperature, and the more remarkable the temperature effect becomes. The smaller temperature dependence of the G mode in whiskers indicates that the graphite whisker has a larger crystal planar domain size than CHOPG with laser annealing at 850 K.[36]

Study of the anti-Stokes spectra in comparison to the Stokes spectra provides much new information about the phonon dispersion effect of graphite materials.[3,12,13] Different frequencies between the Stokes and anti-Stokes Raman signals are observed for the D mode and other modes in graphite whisker similar to the observed results in other graphite materials, such as HOPG (Ref. 12) and carbon nanotubes.[13] All the data about the frequency differences $\Delta\omega$ (defined as $|\omega_{as}|-|\omega_s|$) between the Stokes (s) and anti-Stokes (as) Raman signals of the Raman modes in graphite whiskers excited by 632.8 nm laser excitation along with their energy dispersion of the Stokes Raman modes are summarized in Table III, including the $\Delta\omega$ value of the overtone of L_1 mode and the combination of the L_1 and L_2 modes in a graphite whisker.

The results of the *frequency discrepancy between the Stokes and corresponding anti-Stokes lines* (FDSA) of graphite whiskers are very similar to that of CHOPG.[12] First, the type of FDSA in a whisker can be divided into three categories: the Raman frequencies of the anti-Stokes lines in whiskers are upward shifted (L_1, L_2, D, D', L_1+G, L_2+G, $2D$, and $2D'$ modes), insensitive (G mode), and downward shifted (D'', $D''+D$ modes) relative to those of Stokes lines. Second, Table III clearly shows that the frequency difference ($\Delta\omega$) of a Raman mode has the same sign (positive, negative, and zero) as the energy dispersion of the Raman mode. For the D' and $2D'$ modes in CHOPG and HOPG,[12] the frequency of the D' and $2D'$ modes at the Stokes side is equal to that at the anti-Stokes side, as the Raman theory predicts, because their frequencies are insensitive to the excitation energy. But in graphite whiskers, the positive value for the FDSA of D' and $2D'$ modes can be attributed to their positive frequency dependence on the excitation energy. The above results give evidence for the close physical relationship between the FDSA and the energy dispersion in the Raman spectra of graphite materials.

The FDSA values of higher-order bands in whiskers do not follow those of the fundamentals. For example, the value of the frequency difference $\Delta\omega$ (34 cm^{-1}) for the overtone of the D mode is about *4 times* as large as that (9 cm^{-1}) of the D mode. It seems to contradict the fact that the values of the energy dispersion and the temperature dependence of higher-order bands are almost equal to the sum of those values of its fundamentals. However, we find that the different frequency shifts between the Stokes and anti-Stokes sides of Raman modes in graphite whisker can be predicted by the product between the phonon energy of Raman modes and the value of their energy dispersions as an empirical formula of

TABLE III. The experimental ($expt$) and theoretical (th) frequency difference between the Stokes (s) and anti-Stokes (as) Raman lines of a graphite whisker excited by 632.8 nm laser excitation, which is defined as $\Delta\omega=|\omega_{as}|-|\omega_s|$. Here ω_s and $\partial\omega/\partial\varepsilon_L$ are the frequency and the energy dispersion of Stokes Raman modes at room temperature, respectively. The energy dispersions of $2L_1$ and L_1+L_2 modes are determined by those of the L_1 and L_2 modes.

Assignment	L_1	L_2	$2L_1$	L_1+L_2	D''	D	G	D'	L_1+G	L_2+G	$D''+D$	$2D$	$2D'$
$\omega_s(cm^{-1})$	228	355	452	570	1130	1333	1582	1618	1833	1951	2462	2662	3237
$\partial\omega/\partial\varepsilon_L(cm^{-1}/eV)$	129	216	258	345	-96	46	0	9	140	224	-35	95	18
$(\Delta\omega)_{expt}$ (cm^{-1})	4	9	15	23	-13	9	0	4	33	53	-9	34	8
$(\Delta\omega)_{th}$ (cm^{-1})	3.6	9.5	14.5	24.4	-13.5	7.6	0	1.8	31.8	54.2	-10.7	31.4	7.2

$$\Delta\omega(|\omega_{as}|-|\omega_s|)=\frac{\omega_s}{8065\ (\mathrm{cm}^{-1}/\mathrm{eV})}\frac{\partial\omega_s}{\partial\varepsilon_L} \tag{9}$$

or

$$\Delta\omega(|\omega_{as}|-|\omega_s|)=E_{\omega_s}\frac{\partial\omega_s}{\partial\varepsilon_L}, \tag{10}$$

where E_{ω_s} is the phonon energy of the Raman peak at ω_s and is defined as $\omega_s/8065$ (cm^{-1}/eV), $\Delta\omega$ and ω_s are in units of cm^{-1}, and E_{ω_s} and $\partial\omega/\partial\varepsilon_L$ in eV and cm^{-1}/eV, respectively. Here 8065 is the conversion factor between eV and cm^{-1}. The theoretically calculated FDSA values of all observed Raman modes in whiskers are listed in Table III. The observed FDSA values of all Raman modes in whiskers are in good agreement with the values calculated with the above formula. It suggests that the frequency discrepancy of a Raman mode in graphite materials originates from the dispersive effect of the Raman mode.

Equations (9) and (10) show that the FDSA value of a Raman mode in whiskers is equal to the frequency value covered by the *one-phonon* energy of this Raman mode in its frequency versus laser energy curve. Thomsen and Reich[11] recently reported that the double-resonant process is responsible for the observation of the defect-induced *D* mode in graphite and its peculiar dependence on excitation energy. Based on their theoretical model, they calculated the difference in Stokes and anti-Stokes frequencies of the *D* mode as $\approx 15\ \mathrm{cm}^{-1}$ (for $\varepsilon_L=2.0$ eV), which is twice as much as the experimental value of $\approx 7\ \mathrm{cm}^{-1}$ observed in CHOPG. From Fig. 4 of Ref. 11, it is found that the calculated frequency dependence of the *D* mode on the excitation energy is not linear in a wide range of excitation energy. The slope for the *D* mode excitation energy dependence calculated by their model is about 50 cm^{-1} near $\varepsilon_L=2.0$ eV, and the calculated FDSA value of the *D* mode using the *two-phonon* energy ($2E_{\omega_s}$) instead of the *one-phonon* energy (E_{ω_s}) of the *D* mode in Eq. (10) is about 16 cm^{-1}, which is very close to Thomsen's theoretical value, and thus the theoretical FDSA value of the *D* mode based on the double-resonant Raman process does show the frequency value covered by the *two-phonon* energy of the *D* mode in its frequency versus laser energy curve, but not the *one-phonon* energy observed in the experiment. Therefore, the double-resonant mechanism is unable to explain the observed discrepancy between the Stokes and anti-Stokes frequencies of the *D* mode. To further understand the experimental results, it is necessary to extend the existing models or to build new models.

Based on the previous mechanisms of resonant Raman process of graphite materials,[9,10] the energy dispersions and the different FDSA values of the *D* and 2*D* modes for different graphite materials such as HOPG, SWNT's, and whiskers indicate that the *D* band and its overtone vibrational spectra excited by a given laser energy correspond to a slightly shifted *k* point relative to the *K* point in the two-dimensional Brillouin zone, since there is a slight difference of the electronic structure and phonon dispersion curves near the *K* point of the two-dimensional graphene Brillouin zone resulting from the different local properties of the geometry such as the different bond length and bond angle of the honeycomb lattice, and the bending and folding of graphite layer. Therefore, it is reasonable to observe the different FDSA values of D'', $D''+D$, and other modes in CHOPG and graphite whisker.

IV. SUMMARY

We synthesized a new type of graphite whiskers using a high-temperature heat-treatment method at a special pressure and measured the Raman spectra of graphite whiskers in the range of 150–7800 cm^{-1} using red, green, and blue laser excitation. The intensity of the 2*D* overtone is found to be about 10 times stronger than that of the *G* mode. Because of the very strong enhancement of the 2*D* mode, high-order Raman bands up to fifth order at $\sim 7500\ \mathrm{cm}^{-1}$ have been observed. The energy dispersion of the *D* mode and *G* mode is very similar to that of highly oriented pyrolytic graphite. In contrast to the Raman spectra of HOPG and other graphite materials, two laser-energy-dependent Raman lines are revealed in the low-frequency region of Raman spectra of graphite whiskers, which are believed to be the resonantly enhanced phonons in the transverse-acoustic and longitudinal-acoustic phonon branches. Moreover, the obvious energy dispersion of the D' mode is observed in graphite whiskers.

Polarized micro-Raman spectroscopy has been performed on an individual graphite whisker. The measured results show the maximum intensity of all Raman modes when the whisker is aligned perpendicular to the polarization of the incident excitation and the angular dependence with the incident and scattered light either perpendicular (*HV*) or parallel (*VV*) to one another is in agreement with the theoretically calculated results of a Raman mode with E_{2g} symmetry. According to the polarization effect, the frequency matches, and laser-energy dependence of the Raman modes, we clarify the symmetry type and the assignment of all observed Raman modes in the graphite whisker.

The study of the frequency discrepancy of the Raman modes in graphite whiskers between their Stokes and anti-Stokes components shows that the frequency discrepancy of a Raman mode in graphite materials originates from the dispersive effect of the Raman mode, and the value of the different frequency shift of the Raman mode between its Stokes and anti-Stokes sides in graphite materials is equal to the frequency value covered by the *one-phonon* energy of this Raman mode in its frequency versus laser energy curve, which is the product of the one-phonon energy of this mode and the value of its laser-energy dispersions. The results shows that the double-resonant mechanism is unable to explain the observed discrepancy between the Stokes and anti-Stokes frequencies of the *D* mode, and it is necessary to extend the existing models or build new models to further understand the experimental results.

ACKNOWLEDGMENT

One of the authors (P.H.T.) gratefully acknowledges Professor HeXiang Han for useful discussions.

*Electronic address:
pinghengtan@hotmail.com, phtan@red.semi.ac.cn

[1] M. S. Dresselhaus and G. Dresselhaus, in *Light Scattering in Solids III*, edited by M. Cardona and G. Güntherodt (Springer, Berlin, 1982).
[2] P. C. Eklund, J. M. Holden, and R. A. Jishi, Carbon **33**, 959 (1995).
[3] M. S. Dresselhaus and P. C. Eklund, Adv. Phys. **49**, 705 (2000).
[4] A. Jorio, G. Dresselhaus, M. S. Dresselhaus, M. Souza, M. S. S. Dantas, M. A. Pimenta, A. M. Rao, R. Saito, C. Liu, and H. M. Cheng, Phys. Rev. Lett. **85**, 2617 (2000).
[5] G. S. Duesberg, I. Loa, M. Burghard, K. Syassen, and S. Roth, Phys. Rev. Lett. **85**, 5436 (2000).
[6] Y. Kawashima and G. Katagiri, Phys. Rev. B **59**, 62 (1999).
[7] R. P. Vidano, D. B. Fishbach, L. J. Willis, and T. M. Loehr, Solid State Commun. **39**, 341 (1981).
[8] Y. Wang, D. C. Aolsmeyer, and R. L. McCreery, Chem. Mater. **2**, 557 (1990).
[9] I. Pócsik, M. Hundhausen, M. Koós, and L. Ley, J. Non-Cryst. Solids **227**, 1083 (1998).
[10] M. J. Matthews, M. A. Pimenta, G. Dresselhaus, M. S. Dresselhaus, and M. Endo, Phys. Rev. B **59**, R6585 (1999).
[11] C. Thomsen and S. Reich, Phys. Rev. Lett. **85**, 5214 (2000).
[12] P. H. Tan, Y. M. Deng, and Q. Zhao, Phys. Rev. B **58**, 5453 (1998).
[13] S. D. M. Brown, P. Corio, A. Marucci, M. S. Dresselhaus, M. A. Pimenta, and K. Kneipp, Phys. Rev. B **61**, R5137 (2000).
[14] M. Endo, R. Saito, M. S. Dresselhaus, and G. Dresselhaus, in *Carbon Nanotubes Preparations and Properties*, edited by T. W. Ebbesen (CRC Press, New York, 1997).
[15] R. Bacon, J. Appl. Phys. **31**, 283 (1960), and references therein.
[16] J. A. Floro, S. M. Rossnagel, and R. S. Robinson, J. Vac. Sci. Technol. A **1**, 1398 (1983).
[17] Y. Gogotsi, J. A. Libera, N. Kalashnikov, and M. Yoshimura, Science **290**, 317 (2000).
[18] H. Murayama and M. Maeda, Nature (London) **345**, 791 (1990).
[19] J. Dong, W. C. Shen, B. F. Zhang, X. Liu, F. Y. Kang, J. L. Gu, D. S. Li, and N. P. Chen, Carbon (to be published).
[20] M. S. Dresselhaus, G. Dresselhaus, P. C. Eklund, R. Saito, and M. Endo, in *Carbon Nanotubes Preparations and Properties*, edited by T. W. Ebbesen (CRC Press, New York, 1997).
[21] J. Dong, Ph.D. thesis, Tsinghua University, 2001.
[22] R. J. Nemanich and S. A. Solin, Phys. Rev. B **20**, 392 (1979).
[23] F. Tuinstra and J. L. Koenig, J. Chem. Phys. **53**, 1126 (1970).
[24] K. Nakamura, M. Fujitsuka, and M. Kitajima, Phys. Rev. B **41**, 12 260 (1990).
[25] R. Loudon, Adv. Phys. **13**, 423 (1964).
[26] G. Compagnini and G. Baratta, Appl. Phys. Lett. **61**, 1796 (1992).
[27] R. A. Jishi and G. Dresselhaus, Phys. Rev. B **26**, 4514 (1982).
[28] M. Cardona, in *Light Scattering in Solids II, Basic Concepts and Instrumentation*, edited by M. Cardona and G. Güntherodt (Springer-Verlag, Berlin, 1982).
[29] Y. Kawashima and G. Katagiri, Phys. Rev. B **52**, 10 053 (1995).
[30] W. Z. Li, H. Zhang, C. Y. Wang, Y. Zhang, L. W. Xu, K. Zhu, and S. S. Xie, Appl. Phys. Lett. **70**, 2684 (1997).
[31] P. H. Tan, Y. Tang, Y. M. Deng, F. Li, Y. L. Wei, and H. M. Cheng, Appl. Phys. Lett. **75**, 1524 (1999).
[32] A. C. Ferrari and J. Robertson, Phys. Rev. B **61**, 14 095 (2000).
[33] R. A. Jishi, L. Venkataraman, M. S. Dresselhaus, and G. Dresselhaus, Chem. Phys. Lett. **209**, 77 (1993).
[34] M. S. Dresselhaus, G. Dresselhaus, K. Sugihara, I. L. Spain, and H. A. Goldberg, *Graphite Fibers and Filaments*, Vol. 5, Springer Series in Materials Science (Springer-Verlag, Berlin, 1998).
[35] R. Saito, T. Takeya, T. Kimura, G. Dresselhaus, and M. S. Dresselhaus, Phys. Rev. B **57**, 4145 (1998).
[36] P. H. Tan, Y. M. Deng, Q. Zhao, and W. C. Cheng, Appl. Phys. Lett. **74**, 1818 (1999).